Computational Materials Science 182 (2020) 109791

Contents lists available at ScienceDirect

Computational Materials Science

journal homepage: www.elsevier.com/locate/commatsci

Control of asymmetric track geometry in printed parts of stainless steels, nickel, titanium and aluminum alloys

T. Mukherjee, T. DebRoy*

Department of Materials Science and Engineering, The Pennsylvania State University, University Park, PA 16802, USA

ARTICLE INFO

Keywords:
Additive manufacturing
Powder bed fusion
Heat transfer and fluid flow
Peclet number
Marangoni number
Fourier number

ABSTRACT

In powder bed fusion, distorted temperature fields and deposit dimensions, undesirable surface features, and defects have been attributed to asymmetry in track geometry. It is also thought to affect sensing and control. While data on the asymmetry have been widely reported in the literature for many commonly used alloys, the origin of the asymmetry and the role of alloy composition and process variables are not known. Here we examine the role of local differences in heat transfer from the fusion zone as the origin of asymmetry in the track geometry. We use a mechanistic model of heat transfer and experimental data to examine the role of main process variables and alloy composition on the extent of asymmetry and provide easy-to-use process maps. We show that high laser power and slow scanning speed decreases asymmetry. Marangoni, Fourier and Peclet numbers can be used for controlling asymmetry. Among the four alloys examined, stainless steel 316 and AlSi10Mg are the most and least susceptible to asymmetry because of their lowest and highest thermal diffusivity, respectively.

1. Introduction

In laser-assisted powder bed fusion (PBF-L), a laser beam selectively melts thin layers of alloy powders which after solidification take the shape of the desired track geometry [1,2]. The fusion zone geometry is of critical importance because it affects temperature distribution, local cooling rates, solidification growth rates, and the grain structure and may cause lack-of-fusion voids [3,4,5,6]. Depending on the process conditions and alloys used, the geometry of the deposited track can be asymmetric where the left side of the fusion zone geometry can differ from that of the right side [7–13].

Asymmetry in the track geometry has been observed in PBF-L by several researchers. For example, asymmetry was found in PBF-L of stainless steel 316, which affected the orientation of columnar grains [7]. Asymmetry in PBF-L of stainless steel 316 was also observed by Foroozmehr et al. [10]. Temperature distribution and final deposit dimensions were found to be significantly affected by the asymmetry in the PBF-L of commercially pure iron [12]. Unwanted surface features that may affect the dimensional accuracy and surface roughness and small voids were found in the PBF-L of Ti-6Al-4V because of the track asymmetry [11]. Asymmetry in the track geometry was found to affect solidification parameters during the PBF-L of Inconel 718 [9]. Khan et al. [8] reported asymmetry in the track geometry in the PBF-L of AlSi10Mg. In all aforementioned examples, it is proved that the asymmetry in the track geometry originates because of the differences in thermophysical properties of the solid deposit and powder layer at two sides of the molten pool. For example, a depositing track that has already solidified track at one side and powder layer on the other side can exhibit asymmetry because of non-uniform heat transfer to the two sides. However, the effects of process variables such as laser power, scanning speed, layer thickness, hatch spacing, and powder packing efficiency of the bed on asymmetry are unknown. Furthermore, the relative susceptibilities of various alloys to asymmetry are also not known. As a result, there is no foundation to anticipate and control the extent of asymmetry based on scientific principles.

The origins of this asymmetry are not known, but the local differences in the heat transfer from different locations of the fusion zone is potentially an important factor [11]. For example, one side of the fusion zone may be in contact with a solidified track and the other side may be immersed in a bed of powder with a very different thermal diffusivity. Since the asymmetry changes the surface area, it would also affect any process control that is based on sensing of the surface area.

Here, we propose an asymmetry index that depends on the molten pool shape and size to quantify asymmetry in the track geometry during PBF-L. The index is calculated using a well-tested heat transfer and fluid flow model [14]. The calculated values of the index are tested against independent experimental data from the literature. Using the proposed index, we examine the effects of laser power, scanning speed, layer

* Corresponding author.
E-mail address: debroy@psu.edu (T. DebRoy).

https://doi.org/10.1016/j.commatsci.2020.109791
Received 23 March 2020; Received in revised form 9 May 2020; Accepted 10 May 2020

thickness, hatch spacing and packing efficiency of the powder bed on asymmetry for four commonly used AM alloys, stainless steel 316, Inconel 718, Ti-6Al-4V and AlSi10Mg. Maps are presented to demonstrate the effects of laser power and scanning speed for different alloys. The asymmetry is correlated with three commonly used dimensionless numbers that are of specific interest in AM [15], Peclet, Marangoni, and Fourier numbers.

2. Heat transfer and fluid flow model to predict asymmetry

A well-tested, three-dimensional, transient heat transfer and fluid flow model of PBF-L [14] is used to calculate the molten pool shape and size for various alloys and process conditions. The model solves the equations of conservation of mass, momentum and energy [1]:

$$\frac{\partial u_i}{\partial x_i} = 0 \tag{1}$$

$$\rho\frac{\partial u_j}{\partial t} + \rho\frac{\partial (u_i u_j)}{\partial x_i} = \frac{\partial}{\partial x_i}\left(\mu\frac{\partial u_j}{\partial x_i}\right) + S_j \tag{2}$$

where and μ are the density and the viscosity of the alloy, respectively, x_i is the distance along the i direction, u_i and u_j are the velocity components along the i and j directions, respectively, and S_j is the source term for jth equation of momentum conservation. The energy conservation equation can be written as [1]:

$$\frac{\partial h}{\partial t} + \frac{\partial (u_i h)}{\partial x_i} = \frac{\partial}{\partial x_i}\left(\alpha\frac{\partial h}{\partial x_i}\right) - \frac{\partial \Delta H}{\partial t} - \frac{\partial (u_i \Delta H)}{\partial x_i} + S_v \tag{3}$$

where h denotes the sensible heat, α and ΔH are the thermal diffusivity and the latent heat of fusion of the alloy, respectively, t is the time, u_i is the velocity components along the i direction and S_v is the source term in the energy conservation equation. This source term is applied for the volumetric heat source as [14]:

$$S_v = \frac{\xi\eta P}{\pi r^2 t} exp\left[-\frac{\xi(x_b^2 + y_b^2)}{r^2}\right] \tag{4}$$

where P is laser power, η is absorption coefficient, ξ is power distribution factor varies between 1 and 3 [1], r is laser beam radius, x_b and y_b are the distances from the axis of the laser beam along X and Y directions, respectively and t is the thickness of the powder layer.

The solution domain for the heat transfer and fluid flow model consists of powder bed, substrate, deposited layers and hatches and shielding gas. The boundary conditions for the energy conservation equation are applied as the convective and radiative heat losses from all surfaces of the solution domain [14]:

$$-k\frac{\partial T}{\partial z} = \sigma\varepsilon(T^4 - T_A^4) + h_c(T - T_A) \tag{5}$$

where σ is the Stefan-Boltzmann constant (5.67×10^{-8} Wm^{-2} K^{-4}), k is the thermal conductivity of alloy, ε is the emissivity, h_c is the convective heat transfer coefficient and T_A is the ambient temperature. This model accurately calculates the temperature fields and fusion zone shape and size by considering the effects of convective flow of molten metal. The convective flow is primarily driven by the surface tension variation on the top surface of the molten pool resulting from the spatial gradient of temperature. The resulting stress, called Marangoni shear stress is applied on the top surface of the molten pool as a boundary condition for conservation equation of momentum [1].

The application of the model and the solution procedure are described in detail in our previous publication [14] and are not repeated here. Thermophysical properties of the four alloys, stainless steel 316, Inconel 718, Ti-6Al-4V and AlSi10Mg used in the calculations are taken from the literature [1,16,17] and are provided in Table 1. Since shielding gas is entrapped among the powder particles in PBF-L [16], effective thermophysical properties of the powder bed are different

Table 1
Properties of SS 316, Ti-6Al-4V, IN 718 and AlSi10Mg [1,16,17]. Here 'T' represents temperature in K ranging from ambient to the solidus temperature.

Properties	SS 316	Ti-6Al-4 V	IN 718	AlSi10Mg
Liquidus temperature (K)	1733	1928	1609	867
Solidus temperature (K)	1693	1878	1533	831
Thermal conductivity (W/m K)	$11.82 + 1.06 \times 10^{-2}$ T	$1.57 + 1.6 \times 10^{-2}$ T − 1×10^{-6} T^2	$0.56 + 2.9 \times 10^{-2}$ T − 7×10^{-6} T^2	$113 + 1.06 \times 10^{-5}$ T
Specific heat (J/ kg K)	$330.9 + 0.563$ T − 4.015×10^{-4} T^2 + 9.465×10^{-8} T^3	$492.4 + 0.025$ T − 4.18×10^{-6} T^2	$360.4 + 0.026$ T − 4×10^{-6} T^2	$536.2 + 0.035$ T
Density (kg/m^3)	7800	4000	8100	2670
Latent heat of fusion (J/kg)	272×10^3	284×10^3	209×10^3	423×10^3
Viscosity (kg/m s)	7×10^{-3}	4×10^{-3}	5×10^{-3}	1.3×10^{-3}
dγ/dT (N/m K)	-0.40×10^{-3}	-0.26×10^{-3}	-0.37×10^{-3}	-0.35×10^{-3}
Absorption coefficient in liquid (η_l)	0.3	0.3	0.3	0.3
Absorption coefficient in powder (η_p)	0.7	0.7	0.7	0.7

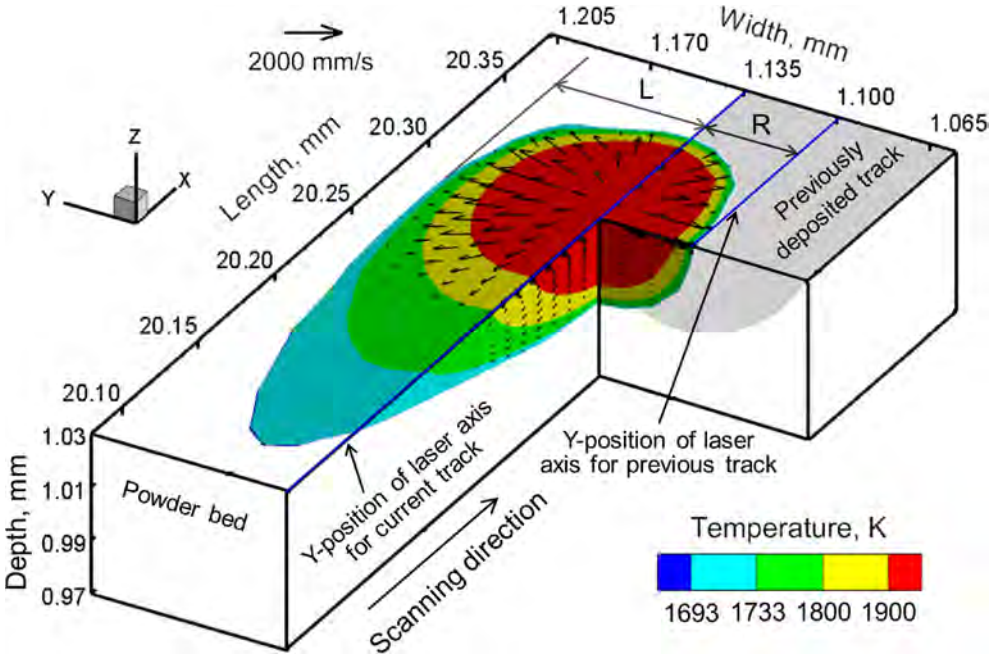

Fig. 1. 3D isometric cut-view of the molten pool during PBF-L of SS 316 using 60 W laser power, 1000 mm/s scanning speed and 30 μm layer thickness. Laser beam axis positions for the previous and current tracks are at y = 1.10 mm and y = 1.135 mm respectively with a 35 μm of hatch spacing between them. The colored contours represent the isotherm indicated in the contour index. Previously deposited track is shown by grey color. Scanning direction is along the positive X-axis. 'R' represents the distance of the right side (side of the previous track) of the molten pool from the laser beam axis (y = 1.135 mm). 'L' represents the distance of the left side (side of the powder layer) of the molten pool from the laser beam axis. L > R indicates asymmetry in the track.

from those of the bulk material and are calculated using the formulae provided in the literature [18,19]. The calculations are performed in a Cartesian coordinate system where scanning, hatching and building directions are along X, Y and Z-axis respectively. The calculations are done using an in-house Fortran code compiled using an Intel Fortran compiler. The calculation time is approximately 5 h for a 20 mm long, 5 layers, 5 hatches build in a personal computer with a 3.40 GHz i7 processor and 8 GB RAM.

3. Results and discussions

Fig. 1 shows the 3D isometric cut-view of the molten pool during PBF-L of SS 316. The boundary of the molten pool is represented by the solidus temperature (1693 K) isotherm. Velocity vectors representing the convective flow inside the molten pool are shown using black arrows whose magnitude can be evaluated by comparing their lengths with that of the reference vector shown in the top left hand side of the figure. The flow of liquid metal is radially outward from the center to the periphery of the molten pool.

It is evident from Fig. 1 that the distance of the left side of the pool from the beam axis (L) is larger than that of the right side (R). In PBF-L, heat conduction through the powder bed is slower than that through the solid deposit because of the lower thermal conductivity of the powder bed due to interparticle void space filled with shielding gas among the powder particles [16,20,21]. At the right side of the pool, heat flows through the already deposited solid track at a faster rate than the left side due to the higher thermal conductivity of the solid deposit than the powder layer. This inequality in the rate of heat transfer at the two sides of the molten pool results in an asymmetry. Here, to quantify the asymmetry, we propose the following index,

$$A^* = \frac{\text{Maximum "half-width" measured from the laser beam track on molten pool surface}}{\text{Corresponding "half-width" on the other side of the beam track}} \quad (6)$$

For the molten pool shown in Fig. 1, A* equals to L/R. For a symmetric track, the value of A* is one and its value increases with the extent of asymmetry. The values A* calculated using the model are rigorously tested using three different sets of experimental data for PBF-L of SS 316 and IN 718 taken from the literature [7,9,10]. Fig. 2 shows that for all three cases, the calculated values of A* agrees reasonably well with the corresponding experimental data.

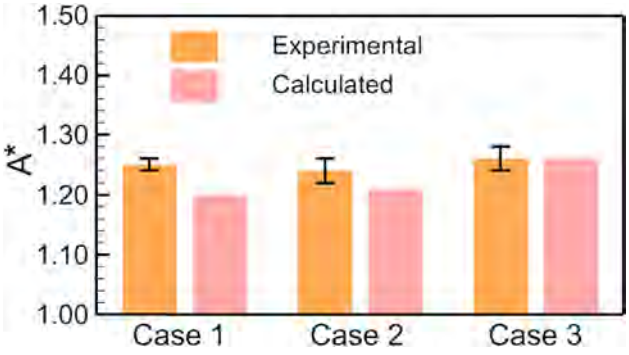

Fig. 2. Comparison between calculated A* and corresponding experimental data from the literature. Case 1 and Case 2 are for SS 316 where experimental data are taken from Andreau et al. [7] and Foroozmehr et al. [10] respectively. Case 3 is for IN 718 where data are taken from Lee et al. [9]. Experimental A* values are estimated from macrograph of the transverse section of the track. Multiple measurements are taken, and errors are represented using error bars in the figure.

Asymmetry depends on the differences in the thermal conductivity of the solid deposit and powder bed. The thermal conductivity of the powder bed depends on the packing efficiency or the compactness of the bed [14,22,23]. Lower packing efficiency indicates more shielding gas entrapped among the powder particles resulting in a low thermal conductivity of the powder bed. In contrast, the thermal conductivity of the powder bed with high packing efficiency approaches that of the solid alloy. Therefore, the thermal conductivity of the powder bed increases with powder packing efficiency as shown in Fig. 3. Rate of heat conduction through a densely packed powder layer with high thermal

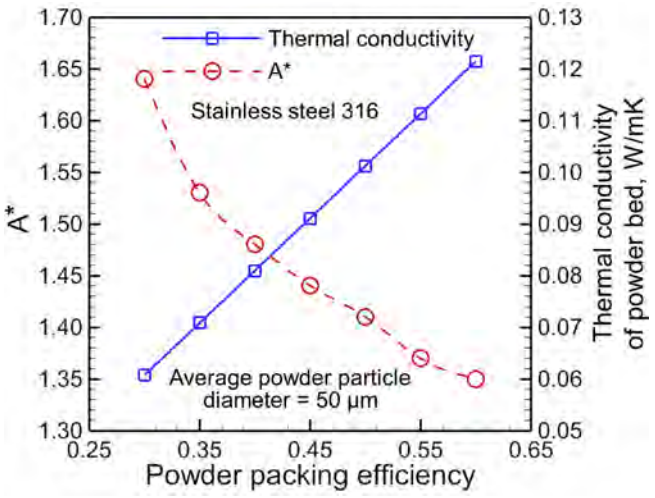

Fig. 3. Variations in the asymmetry index (A*) and thermal conductivity of the powder bed with powder packing efficiency for PBF-L of stainless steel 316 using 60 W laser power, 1000 mm/s scanning speed, 30 μm layer thickness and 35 μm hatch spacing. Thermal conductivity of the powder bed is calculated using the formula provided by Mukherjee et al. [14]. Track length is 20 mm and A* values are calculated at 10 mm from the starting location of the track.

conductivity approaches that through a solid deposit. Therefore, asymmetry in track geometry decreases at high packing efficiency of the powder bed as shown in Fig. 3.

In PBF-L, components are printed by depositing multiple hatches and layers. The differences in heat transfer while depositing different hatches result in changing volume of the molten pool as shown in Fig. 4 (a). During the second hatch, the molten pool dissipates heat rapidly through the already deposited track which has a higher thermal conductivity. As a result, the volume of the molten pool in the second hatch is smaller than that of the first hatch as shown in Fig. 4 (a). However, in the subsequent hatches, the heat transfer pattern remains the same and the molten pool volume does not change significantly. This result is consistent with independent experimental observation available in the literature [11]. For the second and subsequent hatches, asymmetry in the track geometry is observed because of the unequal heat transfer from the molten pool. However, the heat transfer pattern remains the same for the second and subsequent hatches resulting in no appreciable change in the asymmetry as shown in Fig. 4 (a). Fig. 4 (b) shows that the pool volume increases in the upper layers because of reduced rate of heat transfer further away from the substrate. However, after a certain height, pool volume remains unchanged because the heat transfer through the substrate reaches a steady state. The asymmetry depends on the heat transfer conditions on both sides of the molten pool. Therefore, it does not change significantly as more layers are built. A little decrease in the asymmetry with layer, as shown in Fig. 4 (b), is because for larger pool the effect of asymmetry is reduced.

The values of A* for the four alloys under the same processing conditions are compared in Fig. 5 (a). There are two factors that explain the relative susceptibilities of different alloys to the asymmetry. First, alloys with high thermal diffusivity facilitate rapid and uniform heat transfer to the both side of the molten pool which reduces asymmetry. Since SS 316 and AlSi10Mg have the lowest and highest thermal diffusivity among the four alloys, they are the most and least prone to the asymmetry, respectively, as shown in Fig. 5 (a). Second, in a small molten pool the effect of asymmetry is magnified. Fig. 5 (b-d) show that among four alloys, AlSi10Mg has the biggest molten pool due to its

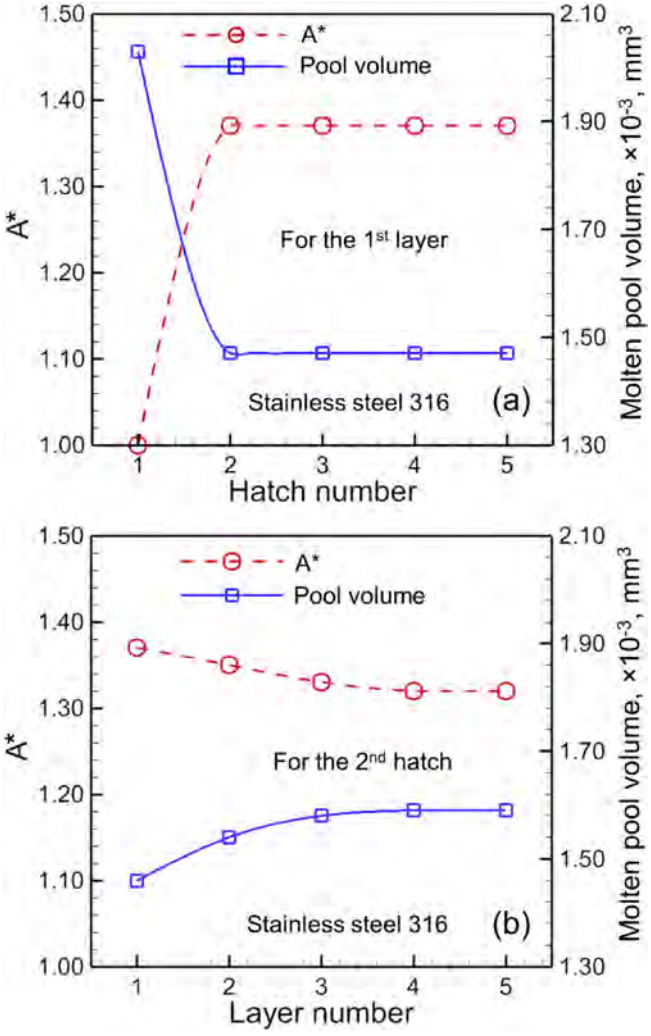

Fig. 4. Variations in the asymmetry index (A*) and pool volume with (a) hatch number and (b) layer number for PBF-L using 60 W laser power, 1000 mm/s scanning speed, 30 μm layer thickness and 35 μm hatch spacing. For all figures track length is 20 mm and A* values are calculated at 10 mm from the starting location of the track.

lowest density and solidus and liquidus temperatures. Therefore, AlSi10Mg is the least susceptible to asymmetry as shown in Fig. 5 (a). In contrast, the figure shows that SS 316 is the most prone to asymmetry due to its smallest pool size among the four alloys.

Fig. 6 (a-d) show the effects of laser power, scanning speed, layer thickness and hatch spacing. From Fig. 5, it is evident that bigger molten pools exhibit less asymmetry. Both slow scanning and high laser power result in bigger molten pool. Therefore, A* decreases at lower scanning speed and higher laser power as shown in Fig. 6 (a). Same observations can be made from the asymmetry maps with respect to varying laser power and scanning speed for SS 316 and AlSi10Mg in Fig. 6 (c) and (d) respectively. Asymmetry in the track geometry originates from unequal heat transfer to the both sides of the molten pool. Varying layer thickness does not significantly alter the heat transfer pattern to the two sides of the molten pool. Therefore, A* does not significantly change with layer thickness as shown in Fig. 6 (b). A small increase in hatch spacing also does not significantly change the heat transfer pattern from the molten pool. Therefore, A* remains almost the

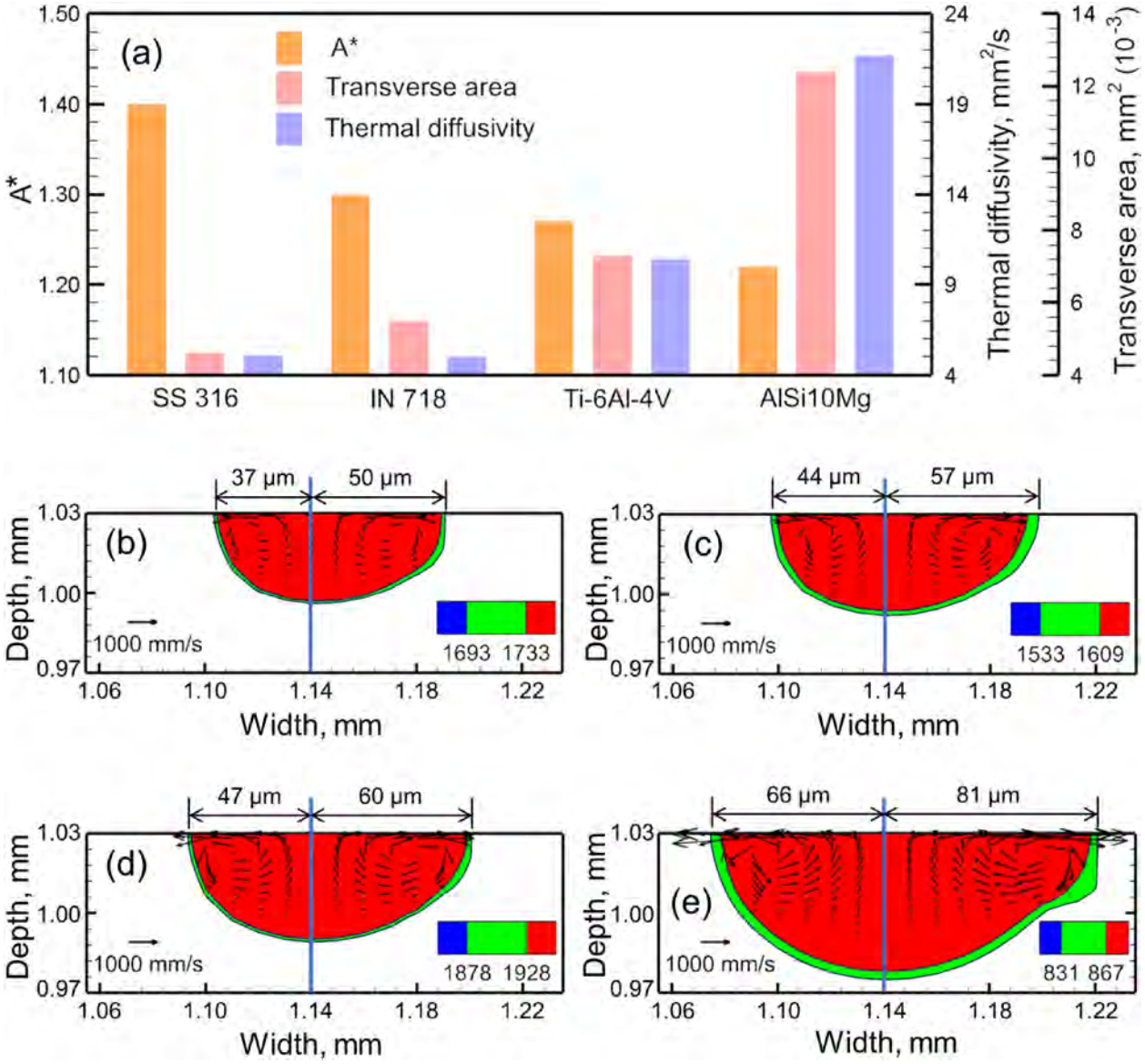

Fig. 5. (a) Comparisons of the asymmetry index (A*), thermal diffusivity at room temperature and transverse area of molten pool for the 1st layer, 2nd hatch for PBF-L of SS 316, IN 718, Ti-6Al-4 V and AlSi10Mg. Molten pool shape and size at transverse plane (YZ plane, refer Fig. 1) for the 1st layer, 2nd hatch for (b) SS 316, (c) IN 718, (d) Ti-6Al-4 V and (e) AlSi10Mg. The results are for 60 W laser power, 1000 mm/s scanning speed, 30 μm layer thickness, 40 μm hatch spacing and 0.5 packing efficiency. The position of the laser beam axis for the second hatch in figures (b-d) is indicated using vertical blue line. The dimensions 'L' and 'R' (refer Fig. 1) are also indicated in figures (b-d). For all figures track length is 20 mm and A* values are calculated at 10 mm from the starting location of the track. In figures (b-d), already solidified material is in the shorter side of the molten pool. (For interpretation of the references to color in this figure legend, the reader is referred to the web version of this article.)

same when the hatch spacing increases from 25 to 65 μm as shown in Fig. 6 (b). However, beyond 65 μm of hatch spacing, two adjacent tracks start to separate from each other which reduces the asymmetry. When the hatch spacing is 105 μm, the two neighboring tracks separate completely from each other and form two symmetrical molten pools with A* = 1.

Shape and size of the pool are often governed by the convective flow of liquid metal. The relative importance of heat transfer by molten metal convection and conduction can be evaluated by the Peclet number [15]:

$$Pe = \frac{U\delta}{\alpha} \tag{7}$$

where U is the characteristic velocity taken as the maximum velocity of the convective flow, δ is the characteristic length which is equal to the maximum width of the molten pool and α is the thermal diffusivity of the alloy. Both U and δ are calculated using the heat transfer and fluid flow model. A high value of Peclet number indicates that convection is the dominant heat transfer mechanism which accelerates heat transfer inside and near the molten pool. Since rapid heat transfer reduces the asymmetry, PBF-L process with high Peclet number is beneficial to minimize the asymmetry for all four alloys as shown in Fig. 7.

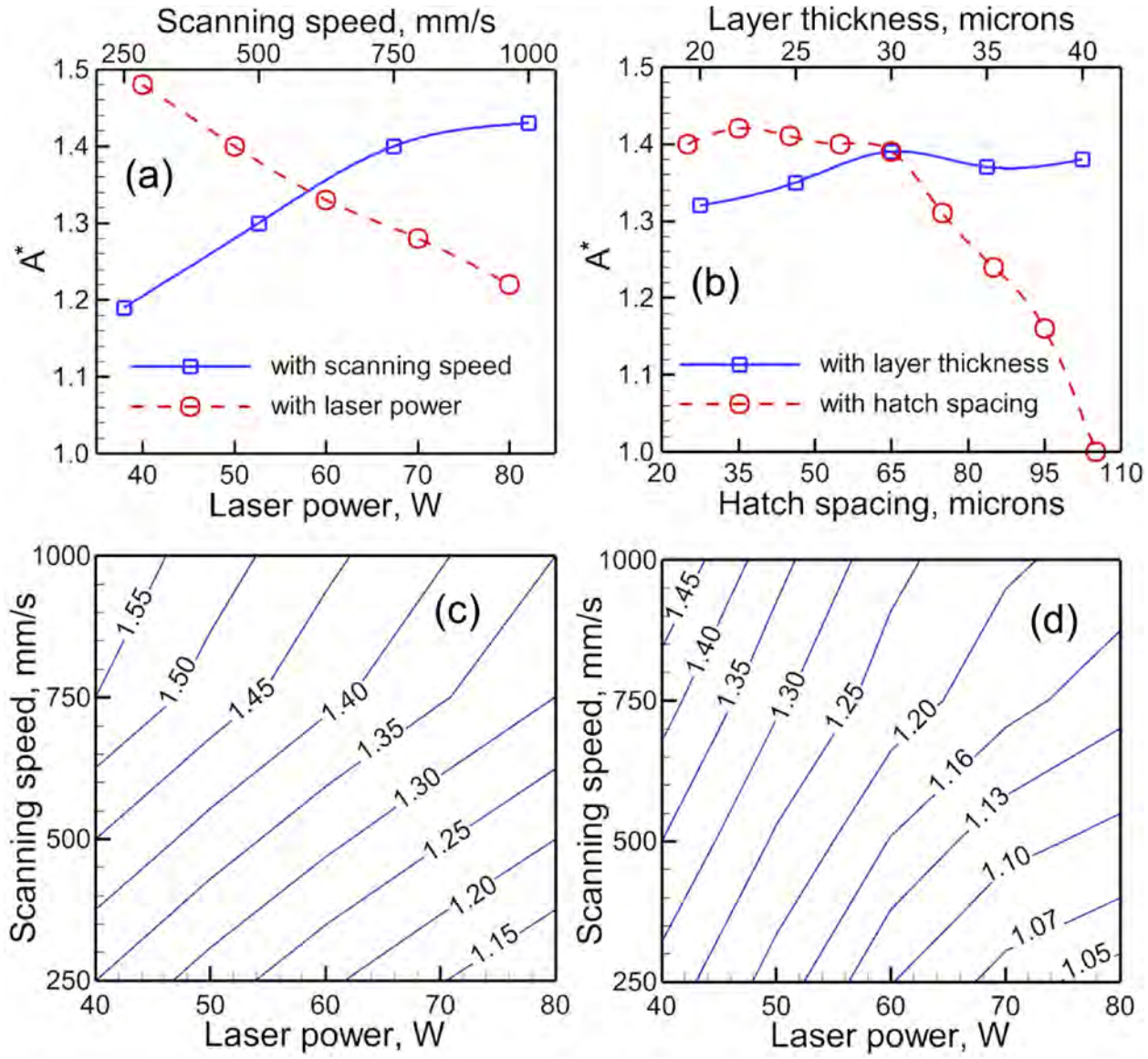

Fig. 6. Variations of the asymmetry index (A*) in the 1st layer, 2nd hatch with (a) laser power and scanning speed and (b) layer thickness and hatch spacing. All results are for PBF-L of stainless steel 316. For figure (a) speed is varied at a constant laser power of 60 W and power is varied at a constant speed of 600 mm/s. However, 30 μm layer thickness, 35 μm hatch spacing and 0.5 packing efficiency are kept constant. For figure (b) layer thickness is varied at a constant hatch spacing of 65 μm and hatch spacing is varied at a constant layer thickness of 30 μm. However, 60 W laser power, 1000 mm/s scanning speed and 0.5 packing efficiency are kept constant. Asymmetry maps for varying laser power and scanning speed for (c) SS 316 and (d) AlSi10Mg at a constant layer thickness of 30 μm, hatch spacing of 35 μm and packing efficiency of 0.5. For all figures track length is 20 mm and A* values are calculated at 10 mm from the starting location of the track.

Convective flow is primarily driven by the spatial gradient of surface tension on the top surface of the molten pool [24,25], also known as the Marangoni stress [1]. Effects of Marangoni stress is represented by the Marangoni number [15,26]:

$$Ma = -\frac{d\gamma}{dT}\frac{\delta \Delta T}{\mu \alpha} \tag{8}$$

where μ and α are the viscosity and thermal diffusivity of the alloy respectively, δ is the characteristic length of the molten pool, which is taken as the maximum width of the molten pool, ΔT is the difference between the peak temperature and the solidus temperature of alloy, and $\frac{d\gamma}{dT}$ is the slope of the surface tension versus temperature plot. For most alloys that do not contain any surface-active elements, such as sulfur and oxygen, $\frac{d\gamma}{dT}$ is negative [27,28]. The peak temperature and pool width required to estimate the Marangoni number are calculated using the heat transfer and fluid flow model. High Marangoni number indicates more rigorous convective flow that accelerates heat transfer inside and near the molten pool. Since rapid heat transfer reduces the asymmetry, PBF-L process with high Marangoni number is beneficial to minimize the asymmetry of the track geometry as shown in Fig. 8 (a). The trend of A* with Marangoni number is consistent for all four alloys.

It is mentioned before that the asymmetry is controlled by the unequal rate of heat transfer from the sides of the molten pool. Fourier number is often used to examine the time needed for a temperature change to occur which indirectly is a measure of the rate of heat transfer in transient situations and is represented as [15,29],

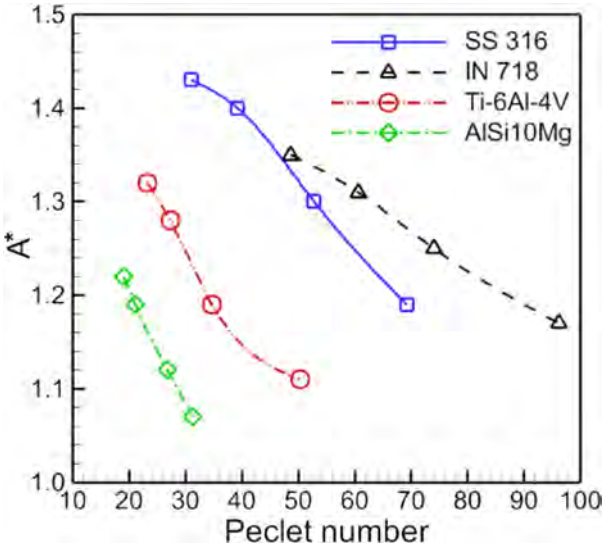

Fig. 7. Variations of the asymmetry index (A*) with Peclet number during PBF-L of four alloys. Data are generated by varying the scanning speed between 250 and 1000 mm/s at laser power of 60 W, 30 μm layer thickness, 35 μm hatch spacing and 0.5 packing efficiency.

$$F = \frac{\alpha}{VL} \tag{9}$$

where α is the thermal diffusivity of alloy, V is the scanning speed and L is the characteristic length which is taken as the depth of the molten pool. High Fourier number indicates rapid heat transfer from the molten pool that minimizes the asymmetry. Based on the results for the four alloys, Fig. 8 (b) shows that the asymmetry in the track geometry decreases with increasing Fourier number. Therefore, from Figs. 7 and 8, it is evident that PBF-L processes with high Peclet, Marangoni and Fourier numbers exhibit lower asymmetry of the track geometry.

4. Summary and conclusions

We examine the conditions for asymmetry of track geometry for four commonly used alloys, SS 316, Inconel 718, Ti-6Al-4 V and AlSi10Mg during powder bed fusion using modeling and experimental results. Below are the specific findings.

1) Alloys with high thermal diffusivity can easily dissipate heat through both the solid deposit and powder layer and exhibit low asymmetry. Among the four alloys considered here, SS 316 and AlSi10Mg are the most and least prone to asymmetry, respectively, because of their lowest and highest thermal diffusivity.
2) Low heat input achieved by reducing laser power or increasing scanning speed results in a smaller molten pool and higher asymmetry. Therefore, asymmetry in the track geometry can be reduced by increasing laser power or reducing scanning speed.
3) PBF-L with a high Fourier number typically achieved by slow scanning speed indicates rapid heat dissipation and reduces asymmetry of the track geometry. High Peclet and Marangoni numbers indicate vigorous convective flow of liquid metal in the fusion zone and reduces asymmetry in the track geometry because of efficient heat transfer.
4) High packing efficiency enhances heat transfer and reduces asymmetry of the track geometry.
5) Heat transfer pattern from the molten pool does not change significantly with varying layer thickness. Therefore, asymmetry in the track geometry cannot be minimized by adjusting layer thickness.

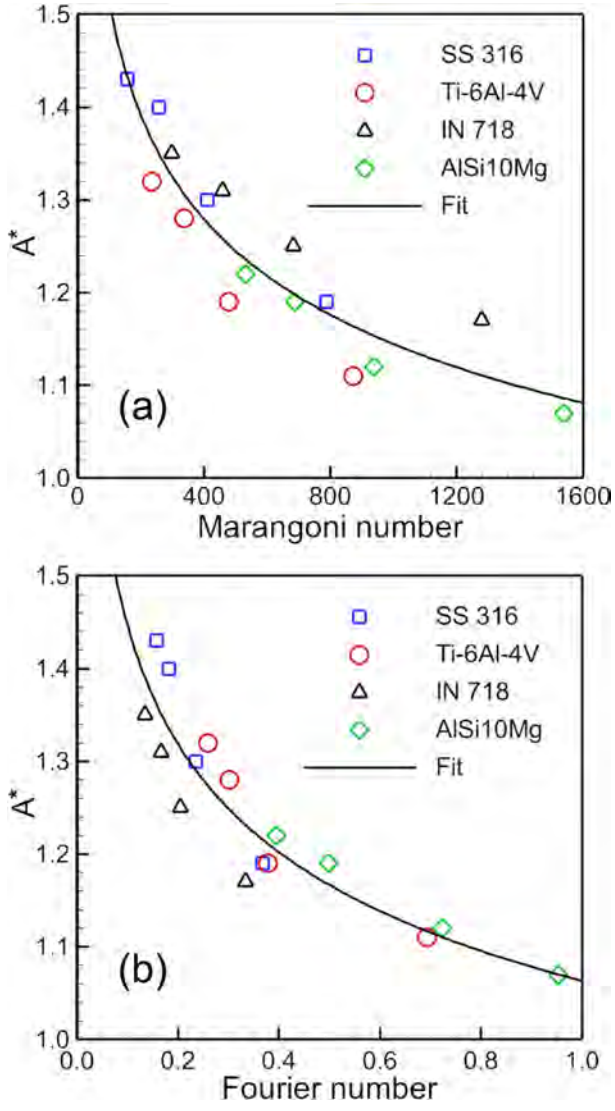

Fig. 8. Variations of the asymmetry index (A*) with (a) Marangoni and (b) Fourier numbers during PBF-L of four alloys. Data are generated by varying the scanning speed between 250 and 1000 mm/s at 60 W power, 30 μm layer thickness, 35 μm hatch spacing and 0.5 packing efficiency.

CRediT authorship contribution statement

T. Mukherjee: Conceptualization, Software, Methodology, Writing - original draft. **T. DebRoy:** Conceptualization, Software, Supervision, Writing - review & editing.

Declaration of Competing Interest

The authors declare that they have no known competing financial interests or personal relationships that could have appeared to influence the work reported in this paper.

Appendix:. Effect of track length on the asymmetry

All results presented in this article are for a track length of 20 mm for consistency. However, it is important to examine if the results are valid for a different track length and this appendix seeks to examine this question. The track lengths are important because the powder bed system is used to make metallic components of various dimensions.

Since the origin of asymmetry can be traced to the unequal heat transfer from the two sides of the fusion zone, it is important to understand how the heat transfer is affected by track length. In a powder bed fusion (PBF) system, heat from a laser beam melts the metallic powders, forms a fusion zone, and heat from the laser beam is transported through the fusion zone to its surroundings. The primary mechanism for heat transfer within the fusion zone is convective heat transfer [14,16]. Since the dimensions of the fusion zone depend on several factors such as laser power, power density distribution, scanning speed, the thermophysical properties of the liquid in the fusion zone, and the thermophysical properties of the surrounding materials. The fusion zone is surrounded by the solidified alloy in the current track. This solid alloy, in turn, is surrounded by the pre-deposited solid track on one side and the powder layer on the other side. The pre-deposited track cools with time. The length of the track and the scanning speed determine the cooling and temperature distribution in the pre-deposited track before the deposition starts at an adjacent hatch. Therefore, the track length affects the heat transfer boundary conditions of the fusion zone indirectly. Since the scanning speed in PBF is very high and the process is highly transient, it is difficult to experimentally determine the fusion zone shape and size in 3D and the temperature profiles and their dependence on track length. Here we use a well-tested 3D, transient numerical heat transfer and fluid flow model [14] to determine the role of track length on the asymmetry of the fusion zone.

Fig. A1 shows computed values of the effect of track length on the asymmetry of the fusion zone geometry. The negligible effect of track length on the asymmetry is primarily because the heat is transported within the fusion zone mainly by convection [14,16] and the convection pattern is not significantly influenced by the temperature in the adjacent pre-deposited track. The variation in heat transfer to the two sides of the molten pool which causes the asymmetry is largely controlled by the differences in the thermophysical properties of the pre-deposited track on one side and the powder layer on the other side of the pool.

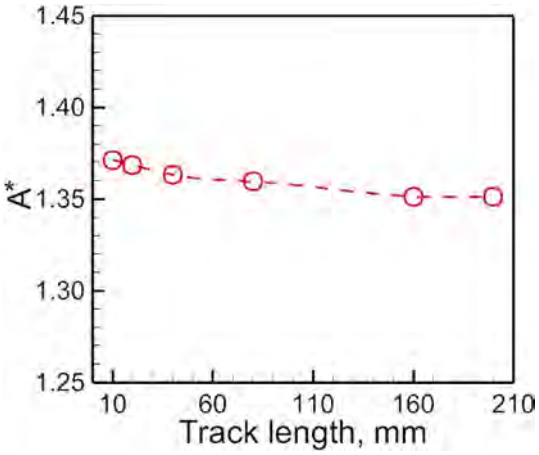

Fig. A1. Variations in the asymmetry index (A*) in the 1st layer, 2nd hatch with track length for PBF-L of SS 316 using 60 W laser power, 1000 mm/s scanning speed, 30 μm layer thickness and 35 μm hatch spacing. A* values are calculated at 8 mm from the starting location of the track.

Data availability statement

The raw/processed data required to reproduce these findings cannot be shared at this time due to technical or time limitations.

References

[1] T. DebRoy, H.L. Wei, J.S. Zuback, T. Mukherjee, J.W. Elmer, J.O. Milewski, et al., Additive manufacturing of metallic components – Process, structure and properties, Prog. Mater. Sci. 92 (2018) 112–224.
[2] T. DebRoy, T. Mukherjee, J.O. Milewski, J.W. Elmer, B. Ribic, J.J. Blecher, W. Zhang, Scientific, technological and economic issues in metal printing and their solutions, Nature Mater. 18 (2019) 1026–1032.
[3] T. Mukherjee, W. Zhang, T. DebRoy, An improved prediction of residual stresses and distortion in additive manufacturing, Comput. Mater. Sci. 126 (2017) 360–372.
[4] T. Mukherjee, T. DebRoy, A digital twin for rapid qualification of 3D printed metallic components, Appl. Mater. Today 14 (2019) 59–65.
[5] J.P. Oliveira, T.G. Santos, R.M. Miranda, Revisiting fundamental welding concepts to improve additive manufacturing: From theory to practice, Prog. Mater. Sci. 107 (2020) 100590.
[6] N.T. Aboulkhair, M. Simonelli, L. Parry, I. Ashcroft, C. Tuck, R. Hague, 3D printing of Aluminium alloys: Additive Manufacturing of Aluminium alloys using selective laser melting, Prog. Mater. Sci. 106 (2019) 100578.
[7] O. Andreau, I. Koutiri, P. Peyre, J.D. Penot, N. Saintier, E. Pessard, T.D. Terris, C. Dupuy, T. Baudin, Texture control of 316L parts by modulation of the melt pool morphology in selective laser melting, J Mater. Process. Technol. 264 (2019) 21–31.
[8] K. Khan, A. De, Modelling of selective laser melting process with adaptive re-meshing, Sci. Technol. Weld. Join. 24 (2019) 391–400.
[9] Y.S. Lee, W. Zhang, Modeling of heat transfer, fluid flow and solidification microstructure of nickel-base superalloy fabricated by laser powder bed fusion, Additive Manufact. 12 (2016) 178–188.
[10] A. Foroozmehr, M. Badrossamay, E. Foroozmehr, S. Golabi, Finite element simulation of selective laser melting process considering optical penetration depth of laser in powder bed, Mater. Des. 89 (2016) 255–263.
[11] T. Craeghs, S. Clijsters, E. Yasa, F. Bechmann, S. Berumen, J.P. Kruth, Determination of geometrical factors in Layerwise Laser Melting using optical process monitoring, Opt. Laser Eng. 49 (2011) 1440–1446.
[12] J. Yin, H. Zhu, L. Ke, W. Lei, C. Dai, D. Zuo, Simulation of temperature distribution in single metallic powder layer for laser micro-sintering, Comp. Mater. Sci. 53 (2012) 333–339.
[13] R.B. Patil, V. Yadava, Finite element analysis of temperature distribution in single metallic powder layer during metal laser sintering, Int. J. Machine Tool. Manufact. 47 (2007) 1069–1080.
[14] T. Mukherjee, H.L. Wei, A. De, T. DebRoy, Heat and fluid flow in additive manufacturing—Part I: Modeling of powder bed fusion, Comp. Mater. Sci. 150 (2018) 304–313.
[15] T. Mukherjee, V. Manvatkar, A. De, T. DebRoy, Dimensionless numbers in additive

manufacturing, J Appl. Phys. 121 (2017) 064904.
[16] T. Mukherjee, H.L. Wei, A. De, T. DebRoy, Heat and fluid flow in additive manufacturing–Part II: Powder bed fusion of stainless steel, and titanium, nickel and aluminum base alloys, Comp. Mater. Sci. 150 (2018) 369–380.
[17] K.C. Mills, Recommended values of thermophysical properties for selected commercial alloys, Woodhead Publishing, 2002.
[18] Y. Zhang, A. Faghri, Melting and resolidification of a subcooled mixed powder bed with moving Gaussian heat source, J. Heat Trans. 120 (1998) 883–891.
[19] M. Rombouts, L. Froyen, A.V. Gusarov, E.H. Bentefour, C. Glorieux, Photopyroelectric measurement of thermal conductivity of metallic powders, J Appl. Phys. 97 (2005) 024905.
[20] T. Mukherjee, T. DebRoy, Mitigation of lack of fusion defects in powder bed fusion additive manufacturing, J Manufact. Process. 36 (2018) 442–449.
[21] M. Markl, C. Körner, Multiscale modeling of powder bed–based additive manufacturing, Ann. Rev. Mater. Res. 46 (2016) 93–123.
[22] W.J. Sames, F.A. List, S. Pannala, R.R. Dehoff, S.S. Babu, The metallurgy and processing science of metal additive manufacturing, Int. Mater. Rev. 61 (2016) 315–360.
[23] D.D. Gu, W. Meiners, K. Wissenbach, R. Poprawe, Laser additive manufacturing of metallic components: materials, processes and mechanisms, Int. Mater. Rev. 57 (2012) 133–164.
[24] S.A. Khairallah, A.T. Anderson, A. Rubenchik, W.E. King, Laser powder-bed fusion additive manufacturing: Physics of complex melt flow and formation mechanisms of pores, spatter, and denudation zones, Acta Mater. 108 (2016) 36–45.
[25] T. Mukherjee, T. DebRoy, Printability of 316 stainless steel, Sci. Technol. Weld. Join. 24 (2019) 412–419.
[26] T. Mukherjee, V. Manvatkar, A. De, T. DebRoy, Mitigation of thermal distortion during additive manufacturing, Scripta Mater. 127 (2017) 79–83.
[27] J. Yin, D. Wang, L. Yang, H.L. Wei, P. Dong, L. Ke, G. Wang, H. Zhu, X. Zeng, Correlation between forming quality and spatter dynamics in laser powder bed fusion, Additive Manufact. 31 (2020) 100958.
[28] H.L. Wei, G.L. Knapp, T. Mukherjee, T. DebRoy, Three-dimensional grain growth during multi-layer printing of a nickel-based alloy Inconel 718, Additive Manufact. 25 (2019) 448–459.
[29] M.V. Elsen, F. Al Bender, J.P. Kruth, Application of dimensional analysis to selective laser melting, Rapid Prototyp. J 14 (2008) 15–22.